Title

The effect of NMDA-R antagonist, MK-801, on Neuronal Mismatch along the Auditory Thalamocortical System

Authors

Gloria G Parras[1,2], MSc; Catalina Valdés-Baizabal[1,2], PhD, Lauren Harms[3], PhD, Patricia Michie[3], PhD & Manuel S Malmierca, PhD [1,2,4]*

Affiliations

[1] Cognitive and Auditory Neuroscience Laboratory, Institute of Neuroscience of Castilla y León (INCYL), Salamanca, Spain.

[2] The Salamanca Institute for Biomedical Research (IBSAL), Salamanca, Spain.

[3] School of Psychology, University of Newcastle, Callaghan, NSW, Australia; Priority Centre for Brain and Mental Health Research, Callaghan, NSW, Australia; Hunter Medical Research Institute, Newcastle, NSW, Australia.

[4] Department of Cell Biology and Pathology, Faculty of Medicine, University of Salamanca, Salamanca, Spain.

Contact Information

* msm@usal.es

ABSTRACT

The predictive coding framework has emerged as an appealing model of mismatch negativity (MMN). It has been repeatedly observed that MMN is reduced in schizophrenia. It is believed that the molecular correlate of this reduction is a NMDA-R hypofunction, a major model of the pathophysiology of schizophrenia. We have previously demonstrated that the neuronal index of mismatch is composed of repetition suppression (RS) and prediction error (PE). Therefore, the main goal of this study was to test how the NMDA-R antagonist, MK-801, affects RS and PE in single units along the rat auditory thalamocortical pathway. Results demonstrate enhanced RS at thalamus and PE at cortex. Moreover, results demonstrate that MK-801 alters the dynamics of adaptation along the thalamocortical axis. These single unit data correlate with the recordings of large-scale responses. This study opens new avenue for future research in the development of safe compounds that target similar binding locations to MK-801.

Keywords: Mismatch negativity, predictive coding, prediction error, repetition suppression, schizophrenia, auditory.

INTRODUCTION

The mismatch negativity (MMN) is an auditory event-related potential (ERP) that occurs when an unexpected stimulus (the deviant, DEV) interrupts a train of expected stimuli (standards, STD) in an *oddball* sequence. The MMN is commonly quantified as the difference between the size of the DEV ERP response and the size of the STD response (1).

The predictive coding framework has emerged as an appealing model of MMN (2) and of how sensory information is processed. According to predictive coding, the brain constantly generates top-down predictions from any regular ascending input that is compared with the actual sensory bottom-up signals. Stimuli that match predictions are suppressed, whereas unexpected stimuli discrepant with the prediction generate an enhanced error signal (3–6). NMDA-R dependent plasticity is believed to underpin the capacity of the brain to adjust internal predictions and use memory of recent past inputs to anticipate future stimuli (7).

There are two likely mechanisms underlying the MMN signal according to the predictive coding model. First, MMN could reflect *repetition suppression*. When the same stimulus is repeatedly presented, neuronal populations originally sensitive to that stimulus undergo adaptation and neural responses decrease (8). The repetition suppression has been conclusively demonstrated in the auditory cortex (AC) of animal models, surface recordings in humans as well as along multiple levels of the auditory hierarchy in rodents, including the inferior colliculus in midbrain and medial geniculate body (MGB) in thalamus (9).

At the same time, MMN could reflect a process of *prediction error*, where the sensory memory of the previously-heard stimuli establishes a predictive model, and the violation of this prediction upon presentation of an unexpected DEV stimuli, results an enhanced neural response that reflects the unexpectedness of the stimuli. Prediction error has been observed in human and rodent surface recordings when suitable control conditions have been included in the design of sound sequences (9–12). Single- and multiunit recordings in the rodent auditory system have demonstrated that prediction error responses are hierarchically organized, from midbrain to auditory cortex, and predominate in non-lemniscal areas (9,13). Therefore, there is strong evidence in both humans and rodents that MMN when extracted as a difference between STD and DEV responses receives contributions from both prediction error and repetition suppression.

MMN is found to be altered in number of different clinical conditions. Most notably, persons with schizophrenia have consistently been observed to have reduced MMN amplitude (14–16). This finding has been replicated in over 100 independent research. For persons with an established illness a large effect size approaching 1 has been observed (15) attesting to the replicability and substantive nature of reduced MMN in schizophrenia. Smaller MMN in schizophrenia has also been found to correlate with impaired cognition, and poorer psychosocial functioning (17,18), leading to the suggestion that MMN may be a useful biomarker for disease progression or risk (19). In humans, acute exposure to the NMDA antagonist ketamine or phencyclidine mimic the full range of schizophrenia symptoms in healthy participants (20), including reduced MMN size (for review see 21). An observation that posits that NMDA hypofunction underlies the neuropathology of the disorder (22). Importantly, schizophrenia-like

impairments and equivalent MMN reduction have been observed after acute administration of NMDA antagonists in animal models (23–26).

Our primary interest in this paper is whether NMDA-R antagonists differentially affect repetition suppression and prediction error. While some studies have demonstrated that MMN-like responses in rodents are altered by NMDA-R antagonists (27–30), only one report has examined the impact of prediction error on the MMN in surface recordings (31). There are no reports that have examined their effects on single-unit activity and local field potential recordings from the thalamus and auditory cortex.

Thus, it is unknown (i) whether there are differential effects of NMDA-R antagonism on prediction error as opposed to repetition suppression at the single unit or local field potential level, and (ii) the regional specificity of where effects of NMDA-R antagonists occur, for example, in the lemniscal *vs*. non-lemniscal auditory areas, or the thalamus *vs*. cortex. Therefore, in the current study, we use an acute exposure to a low dose of MK-801 to examine the impact of NMDA antagonism on individual responses of MGB and AC neurons while auditory oddball, many standards and cascade control sequences were presented (figure 1a-b). This design allowed us to delineate effects on repetition suppression *vs*. prediction error (figure 1c)(9,25,32,33). Our data show that MK-801 produces differential effects on responses to DEV and STD tones in oddball sequences, affecting the mismatch index along the thalamocortical system. Furthermore, we found an increase in repetition suppression in the thalamic regions, while prediction error responses were enhanced in the cortex.

RESULTS

We recorded a total of 290 well isolated neurons, 143 from the control group and 147 from the MK-801-treated group. Since we found no statistically significant differences between the use of the cascade and many-standards sequences for the control group and MK-801 group, except for the MGB_{NL} from the MK-801 group (table 1), the CAS sequence was chosen to control for repetition effects. This is because the CAS paradigm not only controlled for the presentation rate of the deviant stimuli, but also the frequency difference (ascending or descending) between standards and deviants in the oddball sequences.

Effects of MK-801 on the neuronal firing rate. MK-801 injection significantly reduced the responses to STD tones within all regions. By contrast, for responses to the DEV tones, we observed a significant increment in responses in AC but not for the MGB. When the firing rate of the cascade sequence was considered, MK-801 differentially affected the AC and MGB such that CAS responses were significantly increased in the MGB_{NL} but decreased in AC. These results reveal a differential effect of MK-801 on the refractoriness and salience of infrequent events at the single neuron level (Figure 2a, table 2).

Effects of MK-801 on neuronal mismatch and its components. Next we analyzed the differences between these normalized responses and computed three indexes (ranging between -1 and+1): 1) the index of neuronal mismatch (iMM=DEV-STD), similar to the typical SSA index used in previous single neurons studies; 2) the index of prediction error (iPE= DEV-CAS), that shows the relative enhancement of DEV tones compared

with CAS tones and 3) the index of repetition suppression (iRS=CAS-STD) that reflects the level of response suppression due to the repetition effect, and is obtained by comparing the normalized responses to CAS and STD. It should be noted that the iMM is the sum of iRS and iPE (iMM=iRS+iPE).

The analysis of the iMM after the injection of MK-801 demonstrated that iMM values are significantly different from zero for all recording sites (figure 2b, table 1: Friedman test). But when comparisons between groups were considered, the analysis revealed that MK-801 increased the neuronal iMM (figure 2b-iMM; table 2). As described above, these changes are largely due to a reduced response to STD tones in all recording locations and an enhanced response to DEV in the AC.

Since iMM=iRS+iPE, an important advantage of these metrics is that we can determine how much of the mismatch index is due to the regularity of the context (RS) and/or to the occurrence of an infrequent event (PE). Thus, to determine which of these two components of the iMM is affected by MK-801, we computed the indices of iPE and iRS separately.

Interestingly, MGB neurons in the MK-801 group did not show any sign of genuine deviance detection, as iPE values were almost zero and negative. While both AC showed a significant positive iPE (figure 2c; iPE values in table 1). When comparison between groups were analyzed an increased iPE for the MK-801 group in the AC were found, and even a further decreased iPE for the MGB_{NL} in the MK-801 group (figure 2c and e light and bright oranges; iPE in table 2). These data suggest that the MK-801 produces an augmentation of saliency for novel stimuli processed in the AC.

159 Yet, the detection of rare or novel stimuli requires the establishment of a regular context
160 or pattern. Therefore, we were also interested to find out if the refractoriness due to
161 regularity was altered by MK-801. We calculated the iRS by assessing the response of
162 the same tone when it was presented as CAS, with a 10% probability in a regular pattern
163 and presented as STD with a probability of 90%, within an oddball paradigm, so it is in
164 a much more regular context (Harms et al., 2014; Ruhnau et al., 2012). In both cases,
165 we assume some level of regularity adaptation, but only a genuine repetition
166 suppression can be determined if the responses to STD tones are lower than responses
167 to CAS. Our results demonstrate that there is a significant repetition suppression effect
168 in the MK-801 group along the thalamocortical pathway (figure 2d bright blue; iRS in
169 table 1). The analysis also revealed that MK-801 produced a significant increase in
170 repetition suppression at thalamic level but did not affect repetition suppression in the
171 AC when compared with controls (figure 2d-e light and bright blues; results in table 2).

172 These results show that the auditory thalamus and cortex differ in the way repetition
173 effects and prediction errors are processed. To confirm this hypothesis and considering
174 that we have previously found an increase in the level of iPE along the thalamocortical
175 hierarchy in awake and anesthetized animals (Parras et al., 2017), we fitted a linear
176 model to assess if there is a similar increase in iPE along the thalamocortical pathway
177 under MK-801. Using station (MGB and AC) and pathway (Lemniscal *vs.* Non-
178 lemniscal) and their interaction as categorical factors, if MGB_L is used as reference
179 level for these factors, the fitted model is as follows: iPE=-
180 0.131+0.094·NL+0.469·AC+0.091·NL·AC. Next, we applied an ANOVA to this model
181 and found a significant effect of station ($F=196.85$, $p=3.65\times10^{-39}$) and pathway
182 ($F=13.19$, $p=3.02\times10^{-4}$) but not for the interaction ($F=1.54$, $p=0.2138$). A subsequent

post hoc analysis confirmed that the iPE was higher at the MGB_{NL} and AC ($p<0.05$ within all comparisons). These results indicate that indeed, the sensitivity to detect novel stimuli increase significantly along the thalamocortical axis in the MK-801 group (figure 2e, iPE in orange).

Similarly, we also fitted a linear model for iRS in the MK-801 group. The resulting model was: iRS=0.6412-0.0987·NL-0,2753·AC+0.0180·AC·NL. The ANOVA demonstrate a significant effect for both categories (Station F=108.07, $p<0.000$, Pathway F=13.23, $p<0.000$), but not for the interaction (F=0.1211, $p=0.7280$). The *post hoc* comparisons confirmed decreasing levels of repetition suppression as one ascends along the hierarchy from thalamus to cortex and from lemniscal to non-lemniscal [figure 2e, iRS in blue; $MGB_L>MGB_{NL}$ ($p<0.000$), from $MGB_L>AC_L$ ($p<0.000$) and from $MGB_{NL}>AC_{NL}$ ($p<0.000$); but not from AC_L to AC_{NL} ($p=0.0810$)].

In summary, the changes described above demonstrate that NMDA-R antagonism has distinct effects on auditory scene analysis, as measured by the iPE and iRS, at different levels of the thalamocortical hierarchy.

Effect of MK-801 on Spike-Density Function and indexes. Next, we sought to identify how MK-801 affected the temporal responses to auditory stimuli (DEV, STD and CAS) by comparing spike-density functions (SDF) to each condition between groups. Analysis revealed the latency of the main peak for the SDF to DEV tones was mostly unaffected by MK-801 in the MGB, but it was clearly delayed by 40 and 60 ms in the AC_L and AC_{NL}, respectively. Furthermore, the magnitude of the SDF was altered at the AC and MGB_{NL}, with the early component being reduced and the later sustained

component being enhanced (figure 3a, horizontal white line for significant differences at $p<0.05$). When the STD tones were considered, we observed a distinct and significant decrease of the SDF mostly at the AC and only marginally at the subcortical levels (figure 3b). Finally, MK-801 affected mostly the initial responses to cascade tones at all regions, being reduced in the auditory cortex but was earlier and increased in MGB_L (figure 3c). The sustained portion of the SDF was only significantly increased in the MGB_{NL}. Results show that MK-801 has a profound effect on the spike-density functions to DEV, STD and cascade stimuli.

Next, we studied where and when the MK-801 effect on the neuronal indices of iMM, iPE and iRS was significantly different from control. Thus, we examined whether in each group independently (MK-810 and control) these indices are different from zero, *i.e.*, is there a significant iMMN, iPE or iRS at each time point. Figure 3d-f highlights the significant time windows ($p<0.01$) with white and black asterisks for control and MK-801, respectively. The analysis revealed that under MK-801, there was a significant iMM along the thalamocortical axis (between 20-40ms for MGB_L, 20-80ms in MGB_{NL} and from 20-190ms in both AC; Figure 3d, bright purple lines) and a significant iPE between 20 and 180ms in both AC, and a late iPE in the lemniscal thalamus between 60-80ms and 140-190ms (Figure 3e, bright orange lines). We also found significant thalamocortical iRS (figure 3f, bright cyan lines; between 20-40ms for MGB_L, 0-100ms in MGB_{NL}, from 20-120ms in AC_L and between 40-100ms in AC_{NL}).

When we compared the two groups, the analysis revealed that MK-801 produced a significant enhancement of iMM and iPE at both AC subdivisions ($p<0.000$ for iMM between 60-190ms in both AC; and $p<0.05$ for iPE ranging between 100 and 190ms in

229 AC_L and between 60-190ms in AC_{NL}; white horizontal lines in Figures 3 d-f). By
230 contrast, iRS was affected more in the MGB (p<0.000 between 5-35ms in MGB_L;
231 p<0.000 between 40-110ms in MGB_{NL}; p<0.05 between 60-130ms in AC_L; and p<0.05
232 at 80ms in AC_{NL}; white horizontal lines in Figure 3f). Thus, MK-801 produces an
233 increase of iMM and iPE mostly in the late time window in AC, while iRS is much
234 affected in the MGB.

235

236 **MK-801 affects the dynamics of adaptation**. Since MK-801 lowered and flattened
237 responses to STD tones across the response window, we sought to assess the dynamics
238 and the time course of adaptation (figure 4a). Results show that the control group (light
239 gray arrows) exhibit a hierarchical timing for adaptation responses, becoming faster in
240 higher order areas (from top to down, responses reach the half of the initial values at the
241 fourth, ninth, twelfth and fourteenth standard tone, respectively). By contrast, results
242 from the MK-801 group exhibited much faster adaptation dynamics (figure 4b; 50% of
243 the initial response occurred at the third and second standard tones in MGB and AC,
244 respectively; *b* values for control group: MGB_L=-0.1769, MGB_{NL}=-0.4174, AC_L=-
245 0.6824 and AC_{NL}=-1.175; and for MK-801 group: MGB_L=-0.8499, MGB_{NL}=-0.8853,
246 AC_L=-1.712 and AC_{NL}=-1.418).

247 These data reveal that MK-801 alters the timing across the hierarchical organization of
248 the auditory system, resulting in the lemniscal thalamus having almost the same
249 adaptation velocity as the non-lemniscal cortex (arrows in Figure 4b). Furthermore,
250 MK-801 reduces (almost by half) the steady-state plateau in the AC (dotted lines in
251 Figure 4b; *c* values for control group: MGB_L=0.0776, MGB_{NL}=0.2908, AC_L=0.6084

and AC_{NL}=0.7740; and for MK-801 group: MGB_{L}=0.1428, MGB_{NL}=0.2884, AC_{L}=0.3523 and AC_{NL}=0.3834).

All these results together support the idea that MK-801 produces a differential effect on adaptation and deviance detection along the thalamocortical axis, providing new evidence of a change in the firing pattern and temporal responses at single neuron level.

Delayed and broader larger-scaled LFP responses. Next, we wanted to check if the single unit responses correlated with larger-scale measurements of neuronal activity. The analysis of local field potentials (LFP) revealed that MK-801 produced significant changes in MGB_{NL} and AC (both in the lemniscal and non-lemniscal portions) for the deviant, standard and cascade LFPs (Figure 5a-c), such that they exhibited broader and longer responses for DEV-LFP and CAS-LFP in the auditory cortex, while the waveforms of these LFPs were shifted in latency for the MGB_{NL} due to a progressive delay of N1, P1 and N2 (note that this terminology refers to the first negative peak, first positive peak and second negative peak), showing delayed peaks of 8, 14 and 57ms for DEV-LFP and 6, 26 and 45ms delay for CAS-LFP in N1, P1 and N2, respectively (DEV-LFP: N1 peak for MK-801= -6.6μV at 20ms and control= -1.5μV at 12ms; P1 peak for MK-801=6.9μV at 41ms and control=6.8μV at 28ms; finally, N2 peak for MK-801= -5.4μV at 102ms and control= -10.2μV at 45ms. CAS-LFP: N1 peak for MK-801= -6.5μV at 18ms and control= -1.2μV at 12ms; P1 peak for MK-801=5.1μV at 53ms and control= 10.6μV at 27ms; finally, N2 peak for MK-801= -5.0μV at 91ms and control= -10.3μV at 45ms).

Similarly, we also sought significant LFP signals for each computed index (Figure 5d-f). The horizontal colored lines highlight the time at which significant deflections occur to each index-LFP for control and MK-801 groups independently (light and bright horizontal lines, respectively). Additionally, we compared these LFP indices between groups. The analysis of the MM-LFP shows that MK-801 elicited stronger and broader deflections within all regions (horizontal bright purple lines; Figure 5d) and abolished the late negative component (N2) in the AC (MGB_L: N2 = 114-157ms; MGB_{NL}: N1 = 12-21ms, P1 = 32-63ms and N2 = 75-135ms; AC_L: N1 = 10-57ms and P1 = 60-147ms; AC_{NL} N1 = 20-53 and P1 = 60-144ms). Our data also demonstrate that MK-801 produced a higher MM-LFP for virtually the whole LFP response within MGB_{NL} and both AC, while no differences occurred in MGB_L.

Similar to the spike population analysis, and considering that the PE-LFP and RS-LFP both contribute to the MM-LFP, we also wanted to understand how MK-801 shapes the LFP for prediction error and repetition suppression. In response to MK-801, the PE-LFP waveform was reduced at the early component of the MGB_{NL}, while it was increased and delayed for the AC (orange horizontal lines in Figure 5e). Moreover, MK-801 also abolished the N2 deflection (MGB_{NL}: N1 = 99-146ms; AC_L: N1 = 30-65ms and P1 = 87-180ms; AC_{NL} N1 = 30-67 and P1 = 106-180ms). When PE-LFP was compared between groups, we only found differences in AC, mainly at the early (50-70ms) and late components (120-180ms). In other words, the lemniscal thalamus does not exhibit deviance detection, neither at the single neuron level nor at large-scale responses. Hence PE-LFP confirm single unit population data, where MK-801 produced greater levels of deviance detection in the auditory cortex (figure 2e).

Finally, MK-801 had similar effects on RS-LFP to those described above for MM-LFP and PE-LFP, eliciting broader and larger waveforms for MGB_{NL} and AC (Figure 5f; MGB_{NL}: N1 = 10-28ms, P1 = 34-63ms and N2 = 73-108ms; AC_L: N1 = 10-55ms, P1 = 67-140ms and N2 = 148-180ms; AC_{NL}: N1 = 10-51, P1 = 55-132ms and N2 = 141-180ms). When differences between groups are considered, the non-lemniscal thalamus exhibited a shift in the waveform between 15-100ms, while for the cortex, responses over virtually the whole temporal window were increased by MK-801.

DISCUSSION

In this study, we demonstrate that the neuronal index derived from single cell recordings of mismatch is profoundly affected along the auditory thalamocortical system in rats treated acutely with a low dose of the NMDA-R antagonist, MK-801. Importantly, we also reveal that the two elements that make up the index of mismatch negativity, i.e., repetition suppression and prediction error, are differentially affected by MK-801 in single neurons at auditory thalamus and cortex. MK-801 increases repetition suppression in thalamus and prediction error in cortex. The increase in repetition suppression is more prominent in lemniscal areas of the thalamus, while the increase in prediction error is more evident in the non-lemniscal areas of cortex. Furthermore, our results demonstrate that MK-801 alters the dynamics of neuronal adaptation along the thalamocortical axis, becoming faster and stronger especially at thalamic level. These single unit data correlate with the recordings of large-scale responses, LFPs, as they exhibit delayed and broader deflections. In summary, our work demonstrates that the MK-801 increase of the neuronal mismatch in the auditory cortex 60ms after stimulus

onset is due to the combined effect of an increment in the sustained responses to deviant tones and a decrease to standard tones. It should be noted that, in contrast to most previous studies using large scale recording procedures to study neuronal population activity in rodents such as LFPs or EEG via skull screws, we have also recorded single-unit activity, an excellent technique for revealing activity patterns that are present at the single neuron level.

It is well established that NMDA-R plays a fundamental role in neuronal plasticity, controlling long-term potentiation and depression (34). Further, it is generally accepted that human MMN is reduced after NMDA-R antagonist treatments because NMDA-R antagonist blocks synaptic plasticity, precluding the formation of a memory trace for the standard tones (21). As we have seen in our results, MK-801 reduces responses to standard tones thus increasing repetition suppression.

Although this finding supports the hypothesis that NMDA-R antagonists alter sensory-memory formation (35), the findings that low dose (0.1 mg/kg) MK-801 treatment produces a significant increment in the response to the deviant tones, in prediction error and hence, an increment in the neuronal mismatch are in the opposite direction to those expected. It is clear that the role of NMDA-R in the generation of MMN is considerably more complex than thought (36). There have been suggestions in the literature of precedents for our observations. Even considering that MK-801 has 160 times the affinity of ketamine to NMDA-R, necessitating higher ketamine doses for similar drug effect (37), our results conform with those that report an increment in amplitude and latencies to deviant responses after the acute ketamine treatment in rats (38) and with a sub-anaesthetic dose of ketamine in healthy humans producing larger N100 to deviant tones but not MMN (39). Interestingly, a dose response study of the

MK-801 effects on MMR-like responses in male rats showed that while a high dose (0.5mg/kg) reduced late deviance detection (around 55ms), a medium dose (0.3mg/kg) significantly enhanced early deviance detection effects (at about 13 ms) and some evidence of enhanced late effects although not significantly (31). We used a single dose of 0.1mg/kg, as it has been demonstrated that female rats are more sensitive to MK-801 than males (40) and that this dose is enough to induce behavioral/sex effects (41). Importantly, memantine, a low affinity uncompetitive agonist of NMDA-R, has been shown to increase (i) the duration of rodent MMN-like responses (30), (ii) increase MMN amplitude in healthy individuals (42), and (iii) in persons with schizophrenia (43).

The memantine results suggest an interpretation of our findings in terms of the mechanisms underpinning synaptic plasticity (44). Partial blockade of NMDA-R channels (such as mediated by memantine, or low dose MK-801) is also likely to reduce background calcium flux resulting in homeostatic upregulation of NR2B-containing NMDA-Rs leading in turn to the conversion of synapses to a plastic state. That is, while these drugs reduce calcium influx during uncorrelated activity, there is increased calcium influx during correlated activity (produced by physiological stimuli), increased signal to noise, facilitated transmission and increased plasticity (45,46).

Other characteristics of the neuronal mechanisms and microcircuitry involving the glutamate NMDA-R system are relevant to the effects we have observed on the neuronal mismatch after the MK-801 treatment. NMDA-R are located, not only at postsynaptic and presynaptic sites in excitatory neurons, but they are also found at GABAergic inhibitory interneurons in neocortex (47). MK-801 has demonstrated a preferential regulation of the firing rate of cortical GABA interneurons, increasing the

368 firing rate of the majority of pyramidal neurons (48) and therefore producing an
369 imbalance in the excitatory/inhibitory networks in the cortices (49–51). It is well known
370 that cortical GABAergic interneurons differentially amplify stimulus-specific adaptation
371 (a similar phenomenon to iMM) in excitatory pyramidal neurons in auditory cortex (52).
372 Moreover, a model of a mutually coupled excitatory/inhibitory network can explain
373 distinct mechanisms that allow cortical inhibitory neurons to enhance the brain's
374 sensitivity to deviant or unexpected sounds (53). Further MK-801 would alter the tonic
375 inhibitory control of NMDA-R in cortical areas leading to the activation of pyramidal
376 neurons by subsequent deviant tones.

377 The increased repetition suppression we observed in the medial geniculate body
378 can also be by the altered excitatory/inhibitory balance. Although the rat MGB lacks
379 GABAergic neurons, it receives GABAergic input from the thalamic reticular nucleus
380 (TRN) and the inferior colliculus (54,55). The latter is a source of bottom-up inhibitory
381 influences while the TRN provides the MGB with an indirect and inhibitory feedback
382 activation from AC (56). Cortical stimulation hyperpolarizes TRN neurons and
383 increases their inhibitory output to the MGB (57) and furthermore, TRN has been
384 demonstrated to profoundly influence SSA in the MGB (58). Changes in the
385 thalamocortical neuronal firing pattern of thalamic neurons into bursts have been
386 suggested to provide an alerting signal to the cortex to enhance stimulus detection (59).
387 Overall our results match the general concept that when the system is adapted, it is more
388 sensitive to detect changes in the environment (60), where a stronger thalamic repetition
389 suppression (or inhibition) support the increase in the prediction error signals
390 (excitatory) at cortical level, or vice versa. It would be very interesting to test whether

391 thalamic repetition suppression is correlated with cortical prediction error signals, but
392 this question awaits future experiments.

393 Our study is important because it has revealed the involvement of two basic
394 mechanisms, i.e., repetition suppression and prediction error; and two different
395 pathways, lemniscal and non-lemniscal, underlying the neuronal mismatch in the
396 thalamocortical hierarchy. Accordingly, with the predictive coding theory which
397 suggest that the brain is constantly trying to minimize the discrepancy between actual
398 sensory input and internal representations of the environment (4,61). What is new in our
399 data is the critical importance of the hierarchical organization of the auditory system in
400 sharing the 'responsibility' for generating the representation and detecting the
401 discrepancy, largely attributable to thalamic and cortical processes. While altering the
402 balance between the predictive signal and predictive-error signal may underlie the
403 aberrant perception of psychotic disorders (62), our data provide evidence that the
404 NMDA-synaptic plasticity and MMN relationship is not as simple as previously
405 surmised from human studies. Moreover, here we have only tackled the functional role
406 of the NMDA-R under a particular experimental manipulation and we cannot exclude
407 the possibility that larger doses of MK-801 would have generated different results. It is
408 also well known that other neuromodulatory systems such as the dopaminergic,
409 cholinergic and/or cannabinoid systems maybe altered and interact with the NMDA
410 receptors in normal brain function (63,64) and schizophrenia patients (50,65–69). Thus,
411 futures studies of schizophrenia in animal models should also consider these
412 interactions.

413 What are the implications of our findings for schizophrenia? If a safe drug
414 were available that targeted the relevant NMDA-R subunit, and facilitated

415 neuroplasticity as indexed by an increased MMN even for a short time period, it offers
416 opportunities for interventions to remediate cognitive deficits that are a core feature of
417 schizophrenia (70). Memantine which has been shown to increase MMN amplitude in
418 healthy individuals and in schizophrenia has been used as an adjunctive therapy in
419 schizophrenia for some time to improve cognition in particular. While effects of
420 adjunctive therapy are small, recent meta-analysis suggests that there are improvements
421 in global measures of cognition, but improvements in more sensitive composite
422 cognitive test scores were not observed (71). To date, there have been no attempts to
423 utilize MMN response to memantine as an index of neuroplasticity that could be
424 exploited in remediation studies. Interestingly, both the moderate affinity antagonist,
425 memantine, and high affinity antagonist, MK-801, bind to the NR2B subunit of the
426 NMDA-R at very similar binding locations (72) but only memantine has been approved
427 for use in humans given evidence of neurotoxic effects of MK-801 in humans (73). One
428 avenue of future research is the development of safe compounds for human use that
429 target similar binding locations to memantine and MK-801.

430

431 **MATERIAL AND METHODS**

432 Experiments were performed on 48 (control=25; MK-801=23) adult, female Long-
433 Evans rats with body weights between 200-250g (aged 9 to 15 weeks). All experimental
434 procedures were performed at the University of Salamanca, and all procedures and
435 experimental protocols were in accordance with the guidelines of the European
436 Communities Directive (86/609/EEC, 2003/65/EC and 2010/63/EU) and the RD
437 53/2013 Spanish legislation for the use and care of animals. All the details of the study

were approved by the Bioethics Committee of the University of Salamanca (ref# USAL-ID-195).

Surgical procedures: Anesthesia was induced and maintained with urethane (1.5g/kg, i.p), with supplementary doses (0.5g/kg, i.p) given as needed. Dexamethasone (0.25mg/kg) and atropine (0.1mg/kg) were administered at the beginning of the surgery to reduce brain edema and bronchial secretions, respectively. Isotonic glucosaline solution was administered periodically (5-10ml every 6-8h, s.c) to avoid dehydration. During all experimental procedures, animals were artificially ventilated, and CO_2 and temperature monitored (74–77).

The initial procedure was the same in each case, and the subsequent procedures differed only in the craniotomy location, and the placement/orientation for the recording electrode (animals per group/location: control MGB=16, AC=9; MK-801 MGB=15, AC=8). For MGB recordings, a craniotomy (~2x2mm, from -5 to -6.5mm bregma and -3.5mm lateral) was performed in the left parietal bone, dura was removed, and the electrode advanced in a vertical direction (78). For AC recordings, the skin and muscle over the left temporal bone was retracted and a 6x5mm craniotomy was performed (between -2 and -6 from Bregma) over the temporal bone (79) dura was removed and the area was covered with a thin, transparent layer of agar to prevent desiccation and stabilize recordings. Electrodes for AC recording were inserted using a triple axis micromanipulator (Sensapex), forming a 30º angle with the horizontal plane, to penetrate through all cortical layers of the same cortical column.

For this study, animals in MK-801-treated group receive a systemic intraperitoneal injection (0.1mg/kg) of a noncompetitive NMDA-R antagonist (MK-801 hydrogen maleate, M107 Sigma-Aldrich). Control animals did not receive any injection.

Electrophysiological recording procedures. During all procedures, animals were placed in a stereotaxic frame fixed with hollow specula ear bars that housed the sound delivery system. One single neuron and local field potential (LFP) was recorded at a time, using the same tungsten electrode (1-4MΩ) inserted into a single auditory station (MGB or AC) in each individual animal. The signal recorded was pre-amplified (1000x) and band-pass filtered (1-3kHz) with a medusa preamplifier (TDT). This analog signal was digitalized 12k sampling rate and further band-pass filtered (TDT-RX6) separately for spikes (500Hz-3kHz) and LFP (3-50Hz). We used short trains of white noise bursts (30 ms, 5 ms rise-fall ramps) to search for neuronal activity. To prevent neuronal adaptation during the search, some parameters (frequency and intensity) and stimulus type (white noise, pure tone) were manually varied. Once a single neuron was isolated a frequency-response area (FRA) of the response magnitude for each frequency/intensity combination was first computed (Figure 1a). A randomized sequence of pure tones (from 1 to 44 KHz) was presented at a rate of 4Hz, with varying frequency and intensity, and with 3 repetitions of all tones.

For each animal treated with MK-801 the first single neuron was recorded ~15 min after the drug injection (80). Ten evenly-spaced pure tones (0.5 octaves separation) at a fixed sound intensity (usually 20-30dB above the threshold) were selected to each neuron recorded to create the control sequences, cascades and many-standard (9,33), and additionally, adjacent pairs of them were used to present various oddball sequences

(Figure 1b). All sequences were 400 tones in length (75ms duration, 5ms rise-fall ramp and 250ms interstimulus interval), each tone in the control sequences was played 40 times, with the same overall presentation rate as deviants in the oddball sequence.

Oddball sequences were used to test the specific contribution of deviant tones in an adaptation context. An oddball sequence consisted of a repetitive tone (standard 90% probability), occasionally replaced by a tone of a different frequency (deviant 10% probability), in a pseudorandom manner. We used two types of control sequences: the many-standard and cascade sequences. Both containing the same 10 frequencies but differing in the order of presentation. The many-standard control was randomly presented, mimicking the presentation rate and the unpredictability of the deviant tones. While cascades were played always in the same presentation order, ascending or descending in frequency. Hence the cascade contains a regularity, mimic the presentation rate of deviant sounds but in a predictable context and consequently do not violate a regularity. These four conditions, and by extension responses to them, will be denoted as deviant (DEV), standard (STD), cascade (CAS) and many-standard. Finally, if the neuron could be held for long enough, the same protocol was repeated for different frequencies and/or intensity.

Anatomical location. For MGB recording localization, at the end of each tract and experiment, two electrolytic lesions were made to mark the end and the beginning of the auditory signal (figure 6a). Then, animals were given a lethal dose of sodium pentobarbital and perfused transcardially with phosphate buffered saline (0.5% $NaNO_3$ in Phosphate Buffered Saline) followed by a fixative mix of 1% paraformaldehyde and 1% glutaraldehyde). After fixation and dissection, the brain was cryoprotected in 30%

505 sucrose and sectioned into 40μm slices. Sections were Nissl stained with 0.1% cresyl
506 violet. Recording sites were marked on images from an adult rat brain atlas (81) and
507 neurons that were recorded from were assigned to one of the main divisions of the MGB
508 (dorsal, medial or ventral). This information was complemented and confirmed by the
509 stereotaxic coordinates as well as the depth of the neuron within a tract.

510 For the AC experiments, a magnified picture (25x) of the exposed cortex and the
511 Bregma references was taken at the end of the surgery with a digital single lens reflex
512 camera (D5100, Nikon) coupled to the surgical microscope (Zeiss). The picture was
513 overlapped to guide and mark each electrode placement into a micrometric grid (250-
514 500 ~μm spacing; figure 6b). Then we performed several tracts recording multi-unit
515 activity frequency response area (FRA), the characteristic frequency arise from each
516 FRA was placed over the picture, resulting in a characteristic frequency map of each
517 animal. Boundaries were identify following the changes in the tonotopic gradient: high-
518 frequency reversal between the ventral and anterior auditory fields (rostrally), low-
519 frequency reversal between primary and posterior auditory field (dorsocaudally) and
520 high-frequency reversal between ventral and suprarhinal auditory field (ventrally) (79).
521 Then, each recording was located in one of these five fields. Nevertheless, the map was
522 complemented during all electrophysiological recording session with the characteristic
523 frequency of each new tract.

524

525 **Statistical analysis.** All the data analyses were performed with MatlabTM software,
526 using the built-in functions, the Statistics and Machine Learning toolbox, or custom
527 scripts and functions developed in our laboratory. To test for significant excitatory

responses to tones we used a Monte Carlo approach, simulating 1000 peri-stimulus time histogram (PSTH) using a Poison model with a constant firing rate equal to the spontaneous firing rate. A null distribution of baseline-corrected spike counts was generated from this collection of PSTH. Lastly, the *p* value of the baseline-corrected spike count was empirically computed as $p = (g+ 1)/(N+ 1)$, where g is the count of null measures greater than or equal to baseline-corrected spike count, and N=1000 is the size of the null sample. Finally, we only included in the analysis neuron/frequency combinations with significant excitatory response ($p > 0.05$) after the baseline-corrected spike count to at least one of the conditions (DEV, STD, CAS). PSTH were used to estimate the spike-density function (SDF) over the time, showing action potential density over time (in action potentials per second) from −75 to 250ms around stimulus onset, for the 40 trials available for each tone and condition (DEV, STD, CAS), smoothed with a 6ms gaussian kernel ("ksdensity" function in Matlab) in 1ms steps. The baseline spontaneous firing rate was determined as the average firing rate during the 75ms preceding stimulus onset.

The excitatory response was measured as the area below the SDF and above the baseline spontaneous firing rate, between 0 and 180ms after stimulus onset (positive area patches only, to avoid negative response values). This measure will be referred to as "baseline-corrected spike count".

Baseline-corrected spike count responses of a neuron to the same tone in the three conditions (DEV, STD, CAS) were normalized using the formulas:

$DEV_{Normalized} = DEV/N;$

$STD_{Normalized} = STD/N;$

551 $CAS_{Normalized} = CAS/N;$

552 Where $N = \sqrt{DEV^2 + STD^2 + CAS^2}$, is the Euclidean norm of the vector (DEV, STD,

553 CAS) defined by the three responses. Normalized values were the coordinates of a 3D
554 unit vector ($DEV_{Normalized}$, $STD_{Normalized}$, $CAS_{Normalized}$) with the same direction of the
555 original vector (DEV, STD, CAS), and thus the same proportions between the three
556 response measures. This normalization procedure always results in a value ranging 0–1,
557 and has a straightforward geometrical interpretation.

558 From these normalized responses, indices of neuronal mismatch (iMM), repetition
559 suppression (iRS), and prediction error (iPE) were computed as:

560 $iMM = DEV_{Normalized} - STD_{Normalized};$

561 $iPE = DEV_{Normalized} - CAS_{Normalized};$

562 $iRS = CAS_{Normalize} - STD_{Normalized};$

563 These indices, consequently, always range between −1 and 1, and provide the
564 following quantitative decomposition of neuronal mismatch into repetition suppression
565 and prediction error: iMM = iRS + iPE. To test these indices over time, we divided the
566 whole response into 12 time windows, 20ms width, from -50 to 190ms with respect to
567 the stimulus onset. Then, we compared each time window against zero using a sign-rank
568 test, false discovery rate (FDR=0.1) corrected for the 12 windows.

569 For the analysis of the LFP signal, we aligned the recorded wave to the onset of the
570 stimulus for every trial, and computed the mean LFP for every recording site and
571 stimulus condition (DEV-LFP, STD-LFP and CTR-LFP), as well as the differences

between them, resulting in the three LFP-indices: "neuronal mismatch" (MM-LFP = DEV-LFP – STD-LFP), "prediction error" (PE-LFP = DEV-LFP – CAS-LFP) and "repetition suppression" (RS-LFP = CAS-LFP – STD-LFP). Then, grand-averages were computed for all conditions and auditory station separately. The *p* value of the grand-averaged for the three LFP-indices (MM-LFP, PE-LFP and RS-LFP) was determined for every time point with a two-tailed *t* test (FDR corrected).

Our data set was not normally distributed, so we used distribution-free (non-parametric) tests. These included the Wilcoxon signed-rank test and Friedman test (for baseline-corrected spike counts, normalized responses, indices of neuronal mismatch, repetition suppression and prediction error). Only the difference wave for the LFPs was tested using a *t*-test, since each LFP trace is itself an average of 40 waves. For multiple comparison tests, *p* values were FDR corrected using the Benjamini-Hochberg method. Linear models were used to test for significant average iMM, iPE and iRS within each auditory station. Significant effects of station, pathway, and interactions between them were fitted using the 'fitlm' function in Matlab, with robust options. To estimate final sample sizes required for the observed effects after the initial exploratory experiments, we used the 'sampsizepwr' function in Matlab adjusted for the iPE for each region, to obtain a statistical power of 0.8 for this index. Sample sizes were enlarged with additional experiments until they were just greater than the minimum required (number of points recorded, and the minimum required for each station; see Table 1).

To analyze the time course of adaptation we computed an averaged time course for all the standard stimuli presented. Then, we fitted a power law function with a three parameters model, $y(t)=a\cdot t^{b}+c$, where *a* indicates the responses beginning or the first

595 spike strength; *b* the sensitivity to repetitive stimuli, or the adaptation velocity, and *c* the
596 steady-state response. R^2 values indicated that the model fits very well for standard
597 responses in both groups, explaining between 60% and 78% of the response variability
598 within all regions.

599 To analyze spikes differences between MK-801 and control group we computed the
600 median values for each condition tested (DEV, STD and CAS) and their differences
601 (iMM, iRS and iPE) and calculated a ranksum test. To compare each time window
602 between groups a two-sample *t*-test (from 0 to 200ms, Bonferroni corrected for 200
603 comparisons with family-wise error rate FWER< 0.05) was used for the SDF and LFPs
604 to each stimulus condition and indices, using the 'ttest2' function in Matlab, for every
605 time point.

606 **Data availability.** The data that support the findings of this study are available from the
607 corresponding author on reasonable request.

608

609 **Acknowledgements**

610 We thank Drs. Javier Nieto-Diego and David Perez-Gonzalez for their technical support
611 and constructive criticisms; and Nashat Abumaria and Juanita Todd for advice and
612 constructive comments on the discussion. We also thank Ms. Marianny Janiree Pernía
613 Rosales for helping with the histological photomicrography and Mr. Antonio Rivas
614 Cornejo for the technical support.

Funding

Financial support was kindly provided by the Spanish MINECO (SAF2016-75803-P) and JCYL (SA023P17) to MSM. GGP held a fellowship from the Spanish MINECO (BES-2014-069113) and CVB held a fellowship from Mexican CONACyT (216652). LH was supported by an NHMRC project grant: APP1109283.

Competing interest.

The authors report no competing interests.

REFERENCES

1. Näätänen R, Gaillard AWKWK, Mäntysalo S. Early selective-attention effect on evoked potential reinterpreted. Acta Psychol (Amst). 1978 Jul 1;42(4):313–29.

2. Randeniya R, Oestreich LKL, Garrido MI. Sensory prediction errors in the continuum of psychosis. Schizophr Res. 2018 Jan 1;191:109–22.

3. Carbajal G V, Malmierca MS. The Neuronal Basis of Predictive Coding Along the Auditory Pathway: From the Subcortical Roots to Cortical Deviance Detection. Vol. 22, Trends in Hearing. SAGE Publications; 2018. p. 2331216518784822.

4. Friston K. A theory of cortical responses. Philos Trans R Soc B Biol Sci. 2005;360(1456):815–36.

5. Garrido MI, Kilner JM, Stephan KE, Friston KJ. The mismatch negativity: A

review of underlying mechanisms. Clin Neurophysiol. 2009 Mar 1;120(3):453–63.

6. Michie PT, Malmierca MS, Harms L, Todd J. Understanding the neurobiology of MMN and its reduction in schizophrenia. Biol Psychol. 2016 Apr 1;116:1–3.

7. Wacongne C. A predictive coding account of MMN reduction in schizophrenia. Biol Psychol. 2016;116:68–74.

8. Bendixen A, Roeber U, Schröger E. Regularity extraction and application in dynamic auditory stimulus sequences. J Cogn Neurosci. 2007 Oct 13;19(10):1664–77.

9. Parras GG, Nieto-Diego J, Carbajal G V., Valdés-Baizabal C, Escera C, Malmierca MS. Neurons along the auditory pathway exhibit a hierarchical organization of prediction error. Nat Commun. 2017 Dec 15;8(1):2148.

10. Harms L, Fulham WR, Todd J, Budd TW, Hunter M, Meehan C, et al. Mismatch negativity (MMN) in freely-moving rats with several experimental controls. PLoS One. 2014;9(10):e110892.

11. Kurkela JLO, Lipponen A, Kyläheiko I, Astikainen P. Electrophysiological evidence of memory-based detection of auditory regularity violations in anesthetized mice. Sci Rep. 2018 Feb 14;8(1):3027.

12. Nakamura T, Michie PT, Fulham WR, Todd J, Budd TW, Schall U, et al. Epidural Auditory Event-Related Potentials in the Rat to Frequency and duration Deviants: Evidence of Mismatch Negativity? Front Psychol. 2011;2:367.

13. Carbajal G, Malmierca MS. The unique role of the non-lemniscal pathway on

658 stimulus-specific adaptation (SSA) in the auditory system. Procedings Int Symp
659 Audit Audiol Res. 2018;6(February).

660 14. Bodatsch M, Brockhaus-Dumke A, Klosterkötter J, Ruhrmann S. Forecasting
661 Psychosis by Event-Related Potentials—Systematic Review and Specific Meta-
662 Analysis. Biol Psychiatry. 2015 Jun 1;77(11):951–8.

663 15. Erickson MA, Ruffle A, Gold JM. A Meta-Analysis of Mismatch Negativity in
664 Schizophrenia: From Clinical Risk to Disease Specificity and Progression. Biol
665 Psychiatry. 2016;79(12):980–7.

666 16. Umbricht D, Krljes S. Mismatch negativity in schizophrenia: a meta-analysis.
667 Schizophr Res. 2005 Jul 1;76(1):1–23.

668 17. Light GA, Braff DL. Mismatch negativity deficits are associated with poor
669 functioning in schizophrenia patients. Arch Gen Psychiatry. 2005 Feb
670 1;62(2):127–36.

671 18. Rasser PE, Schall U, Todd J, Michie PT, Ward PB, Johnston P, et al. Gray matter
672 deficits, mismatch negativity, and outcomes in schizophrenia. Schizophr Bull.
673 2011 Jan;37(1):131–40.

674 19. Light GA, Swerdlow NR. Future clinical uses of neurophysiological biomarkers
675 to predict and monitor treatment response for schizophrenia. Ann N Y Acad Sci.
676 2015 May;1344(1):105–19.

677 20. Krystal JH, Perry EB, Gueorguieva R, Belger A, Madonick SH, Abi-Dargham A,
678 et al. Comparative and interactive human psychopharmacologic effects of
679 ketamine and amphetamine: Implications for glutamatergic and dopaminergic

model psychoses and cognitive function. Arch Gen Psychiatry. 2005 Sep 1;62(9):985–95.

21. Todd J, Harms L, Schal l U, Michie PT. Mismatch negativity: Translating the potential. Vol. 4, Frontiers in Psychiatry. Frontiers; 2013. p. 171.

22. Javitt DC, Steinschneider M, Schroeder CE, Arezzo JC. Role of cortical N-methyl-D-aspartate receptors in auditory sensory memory and mismatch negativity generation: implications for schizophrenia. Proc Natl Acad Sci U S A. 1996;93(21):11962–7.

23. Featherstone RE, Melnychenko O, Siegel SJ. Mismatch negativity in preclinical models of schizophrenia. Schizophr Res. 2018 Jan 1;191:35–42.

24. Mouri A, Noda Y, Enomoto T, Nabeshima T. Phencyclidine animal models of schizophrenia: Approaches from abnormality of glutamatergic neurotransmission and neurodevelopment. Neurochem Int. 2007 Jul 1;51(2–4):173–84.

25. Harms L. Mismatch responses and deviance detection in N-methyl-D-aspartate (NMDA) receptor hypofunction and developmental models of schizophrenia. Biol Psychol. 2016 Apr 1;116:75–81.

26. Siegel SJ, Talpos JC, Geyer MA. Animal models and measures of perceptual processing in schizophrenia. Neurosci Biobehav Rev. 2013 Nov;37(9 Pt B):2092–8.

27. Ehrlichman RS, Maxwell CR, Majumdar S, Siegel SJ. Deviance-elicited changes in event-related potentials are attenuated by ketamine in mice. J Cogn Neurosci. 2008 Aug;20(8):1403–14.

28. Sivarao D V, Chen P, Yang Y, Li Y-W, Pieschl R, Ahlijanian MK. NR2B Antagonist CP-101,606 Abolishes Pitch-Mediated Deviance Detection in Awake Rats. Front psychiatry. 2014;5:96.

29. Tikhonravov D, Neuvonen T, Pertovaara A, Savioja K, Ruusuvirta T, Näätänen R, et al. Effects of an NMDA-receptor antagonist MK-801 on an MMN-like response recorded in anesthetized rats. Brain Res. 2008;1203(Haartmaninkatu 8):97–102.

30. Tikhonravov D, Neuvonen T, Pertovaara A, Savioja K, Ruusuvirta T, Näätänen R, et al. Dose-related effects of memantine on a mismatch negativity-like response in anesthetized rats. Neuroscience. 2010 Jun 2;167(4):1175–82.

31. Harms L, Fulham WR, Todd J, Meehan C, Schall U, Hodgson DM, et al. Late deviance detection in rats is reduced, while early deviance detection is augmented by the NMDA receptor antagonist MK-801. Schizophr Res. 2018 Jan 1;191:43–50.

32. Opitz B, Schröger E, von Cramon DY. Sensory and cognitive mechanisms for preattentive change detection in auditory cortex. Eur J Neurosci. 2005 Jan 1;21(2):531–5.

33. Ruhnau P, Herrmann B, Schröger E. Clinical Neurophysiology Finding the right control : The mismatch negativity under investigation. Clin Neurophysiol. 2012;123(3):507–12.

34. Blanke ML, VanDongen AMJ. Activation Mechanisms of the NMDA Receptor (Chapter 13). Biology of the NMDA Receptor. CRC Press/Taylor & Francis;

2009. 283-312 p.

35. Auksztulewicz R, Friston K. Repetition suppression and its contextual determinants in predictive coding. Cortex. 2016;80:125–40.

36. Näätänen R, Paavilainen P, Rinne T, Alho K. The mismatch negativity (MMN) in basic research of central auditory processing: A review. Clin Neurophysiol. 2007 Dec 1;118(12):2544–90.

37. Schuelert N, Dorner-Ciossek C, Brendel M, Rosenbrock H. A comprehensive analysis of auditory event-related potentials and network oscillations in an NMDA receptor antagonist mouse model using a novel wireless recording technology. Physiol Rep. 2018 Aug;6(16):e13782.

38. Ahnaou A, Huysmans H, Biermans R, Manyakov N V., Drinkenburg WHIM. Ketamine: differential neurophysiological dynamics in functional networks in the rat brain. Transl Psychiatry. 2017;7(9):e1237.

39. Oranje B, Berckel B van, Kemner C, Ree J van, Kahn R, Verbaten M. The Effects of a Sub-Anaesthetic Dose of Ketamine on Human Selective Attention. Neuropsychopharmacology. 2000 Mar 1;22(3):293–302.

40. Andine P, Widermark N, Axelsson R, Nyberg G, Olofsson U, Martensson E, et al. Characterization of MK-801-Induced Behavior as a Putative Rat Model of Psychosis. J Pharmacol Exp Ther. 1999;290(3):1393–408.

41. Meehan C, Harms L, Frost JD, Barreto R, Todd J, Schall U, et al. Effects of immune activation during early or late gestation on schizophrenia-related behaviour in adult rat offspring. Brain Behav Immun. 2017 Jul 1;63:8–20.

746 42. Korostenskaja M, Nikulin V V., Kičić D, Nikulina A V., Kähkönen S. Effects of
747 NMDA receptor antagonist memantine on mismatch negativity. Brain Res Bull.
748 2007 May 30;72(4–6):275–83.

749 43. Swerdlow NR, Bhakta S, Chou H-H, Talledo JA, Balvaneda B, Light GA.
750 Memantine Effects On Sensorimotor Gating and Mismatch Negativity in Patients
751 with Chronic Psychosis. Neuropsychopharmacology. 2016 Jan;41(2):419–30.

752 44. Slutsky I, Sadeghpour S, Li B, Liu G. Enhancement of Synaptic Plasticity
753 through Chronically Reduced Ca2+ Flux during Uncorrelated Activity. Neuron.
754 2004 Dec 2;44(5):835–49.

755 45. Abumaria N, Yin B, Zhang L, Li X-Y, Chen T, Descalzi G, et al. Effects of
756 elevation of brain magnesium on fear conditioning, fear extinction, and synaptic
757 plasticity in the infralimbic prefrontal cortex and lateral amygdala. J Neurosci.
758 2011 Oct 19;31(42):14871–81.

759 46. Slutsky I, Abumaria N, Wu L-J, Huang C, Zhang L, Li B, et al. Enhancement of
760 Learning and Memory by Elevating Brain Magnesium. Neuron. 2010 Jan
761 28;65(2):165–77.

762 47. DeBiasi S, Minelli A, Melone M, Conti F, DeBiasi, S., Minelli, A., Melone, M.,
763 & Conti F. Presynaptic NMDA receptors in the neocortex are both auto- and
764 heteroreceptors. Neuroreport. 1996 Nov;7(15–17):2773–6.

765 48. Homayoun H, Moghaddam B. NMDA Receptor Hypofunction Produces
766 Opposite Effects on Prefrontal Cortex Interneurons and Pyramidal Neurons. J
767 Neurosci. 2007 Oct 24;27(43):11496–500.

768 49. Javitt D, Lee M, Kantrowitz J, Martinez A. Mismatch negativity as a biomarker
769 of theta band oscillatory dysfunction in schizophrenia. Schizophr Res.
770 2018;191(2016):51–60.

771 50. Okada M, Fukuyama K, Kawano Y, Shiroyama T, Ueda Y. Memantine protects
772 thalamocortical hyper-glutamatergic transmission induced by NMDA receptor
773 antagonism via activation of system xc. Pharmacol Res Perspect. 2019
774 Feb;7(1):e00457.

775 51. Bygrave AM, Masiulis S, Nicholson E, Berkemann M, Barkus C, Sprengel R, et
776 al. Knockout of NMDA-receptors from parvalbumin interneurons sensitizes to
777 schizophrenia-related deficits induced by MK-801. Transl Psychiatry. 2016 Apr
778 12;6(4):e778.

779 52. Chen I-WI-W, Helmchen F, Lutcke H. Specific Early and Late Oddball-Evoked
780 Responses in Excitatory and Inhibitory Neurons of Mouse Auditory Cortex. J
781 Neurosci. 2015 Sep 9;35(36):12560–73.

782 53. Natan RG, Briguglio JJ, Mwilambwe-Tshilobo L, Jones SI, Aizenberg M,
783 Goldberg EM, et al. Complementary control of sensory adaptation by two types
784 of cortical interneurons. Elife. 2015 Oct 13;4.

785 54. Malmierca MS. The Structure and Physiology of the Rat Auditory System: An
786 Overview. In 2003. p. 147–211.

787 55. Winer JA, Kelly JB, Larue DT. Neural architecture of the rat medial geniculate
788 body. Hear Res. 1999 Apr 1;130(1–2):19–41.

789 56. Bartlett EL. The organization and physiology of the auditory thalamus and its

role in processing acoustic features important for speech perception. Brain Lang. 2013 Jul;126(1):29–48.

57. Crabtree JW, Lodge D, Bashir ZI, Isaac JTR. GABAA, NMDA and mGlu2 receptors tonically regulate inhibition and excitation in the thalamic reticular nucleus. Eur J Neurosci. 2013 Mar;37(6):850–9.

58. Yu X, Xu X, He S, He J. Change detection by thalamic reticular neurons. Nat Neurosci. 2009 Sep 16;12(9):1165–70.

59. Hu H, Agmon A. Differential Excitation of Distally versus Proximally Targeting Cortical Interneurons by Unitary Thalamocortical Bursts. J Neurosci. 2016;36(26):6906–16.

60. Musall S, von der Behrens W, Mayrhofer JM, Weber B, Helmchen F, Haiss F. Tactile frequency discrimination is enhanced by circumventing neocortical adaptation. Nat Neurosci. 2014 Nov 21;17(11):1567–73.

61. Rauss K, Pourtois G. What is Bottom-Up and What is Top-Down in Predictive Coding? Front Psychol. 2013;4:276.

62. Sterzer P, Adams RA, Fletcher P, Frith C, Lawrie SM, Muckli L, et al. The Predictive Coding Account of Psychosis. 2018;

63. Ayala YA, Pérez-González D, Malmierca MS. Stimulus-specific adaptation in the inferior colliculus: The role of excitatory, inhibitory and modulatory inputs. Biol Psychol. 2016;116:10–22.

64. Valdés-Baizabal C, Parras GG, Ayala YA, Malmierca MS. Endocannabinoid Modulation of Stimulus-Specific Adaptation in Inferior Colliculus Neurons of

812 the Rat. Sci Rep. 2017;7(1):1–14.

813 65. Coyle JT, Balu D, Benneyworth M, Basu A, Roseman A. Beyond the dopamine
814 receptor: novel therapeutic targets for treating schizophrenia. Dialogues Clin
815 Neurosci. 2010;12(3):359–82.

816 66. Howes OH, Kaar SJ. Antipsychotic drugs: challenges and future directions.
817 World Psychiatry. 2018 Jun;17(2):170–1.

818 67. Lucatch AM, Coles AS, Hill KP, George TP. Cannabis and Mood Disorders.
819 Curr Addict Reports. 2018 Sep 10;5(3):336–45.

820 68. Musty R., Deyo R., Baer J., Darrow S., Coleman B. Effects of SR141716 on
821 animal models of schizophrenia. InSymposium Cannabinoids, Int Cannabinoid
822 Res Soc Burlington, Vermont. 2000;

823 69. Parr T, Friston KJ. The Anatomy of Inference: Generative Models and Brain
824 Structure. Front Comput Neurosci. 2018;12:90.

825 70. Green MF, Kern RS, Braff DL, Mintz J. Neurocognitive deficits and functional
826 outcome in schizophrenia: are we measuring the "right stuff"?
827 Schizophr Bull. 2000;26(1):119–36.

828 71. Kishi T, Ikuta T, Oya K, Matsunaga S, Matsuda Y, Iwata N. Anti-dementia
829 Drugs for Psychopathology and Cognitive Impairment in Schizophrenia: A
830 Systematic Review and Meta-analysis. Int J Neuropsychopharmacol. 2018 May
831 14;21(8):748.

832 72. Song X, Jensen MØ, Jogini V, Stein RA, Lee C-H, Mchaourab HS, et al.
833 Mechanism of NMDA receptor channel block by MK-801 and memantine.

834 Nature. 2018 Apr 18;556(7702):515–9.

835 73. Olney J, Labruyere J, Price M. Pathological cahnges induced in cerebrocortical
836 neurons by phencyclidine and related drugs. Science (80-). 1989 Apr
837 15;244(4910):1360–2.

838 74. Ayala YA, Malmierca MS. Cholinergic Modulation of Stimulus-Specific
839 Adaptation in the Inferior Colliculus. J Neurosci. 2015;35(35):12261–72.

840 75. Duque D, Malmierca MS. Stimulus-specific adaptation in the inferior colliculus
841 of the mouse: anesthesia and spontaneous activity effects. Brain Struct Funct.
842 2015 Nov 13;220(6):3385–98.

843 76. Duque D, Wang X, Nieto-Diego J, Krumbholz K, Malmierca MS. Neurons in the
844 inferior colliculus of the rat show stimulus-specific adaptation for frequency, but
845 not for intensity. Sci Rep. 2016 Apr 12;6:24114.

846 77. Pérez-González D, Hernández O, Covey E, Malmierca MS. GABA A-mediated
847 inhibition modulates stimulus-specific adaptation in the inferior colliculus. PLoS
848 One. 2012;7(3).

849 78. Antunes FM, Nelken I, Covey E, Malmierca MS. Stimulus-Specific Adaptation
850 in the Auditory Thalamus of the Anesthetized Rat. PLoS One. 2010 Nov
851 19;5(11):e14071.

852 79. Nieto-Diego J, Malmierca MS. Topographic Distribution of Stimulus-Specific
853 Adaptation across Auditory Cortical Fields in the Anesthetized Rat. Zatorre R,
854 editor. PLOS Biol. 2016 Mar 7;14(3):e1002397.

855 80. Vezzani A, Serafini R, Stasi MA, Caccia S, Conti I, Tridico R V, et al. Kinetics

of MK-801 and its effect on quinolinic acid-induced seizures and neurotoxicity in rats. J Pharmacol Exp Ther. 1989 Apr 1;249(1):278–83.

81. Paxinos G, Watson C. The Rat Brain in Stereotaxic Coordinates : Hard Cover Edition. Elsevier Science; 2013. 466 p.

a) Frequency Response Area Example

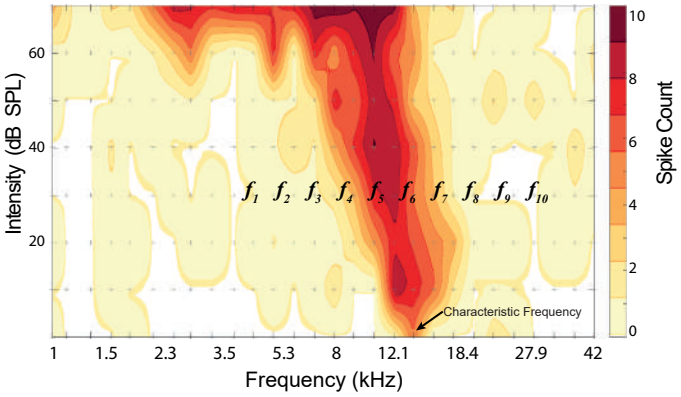

b) Paradigms

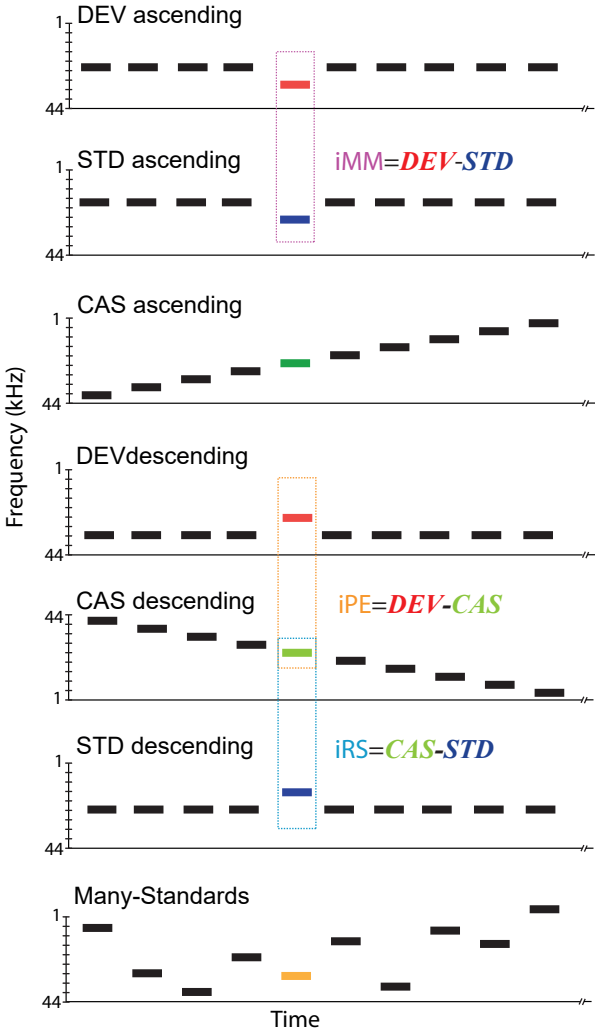

c)

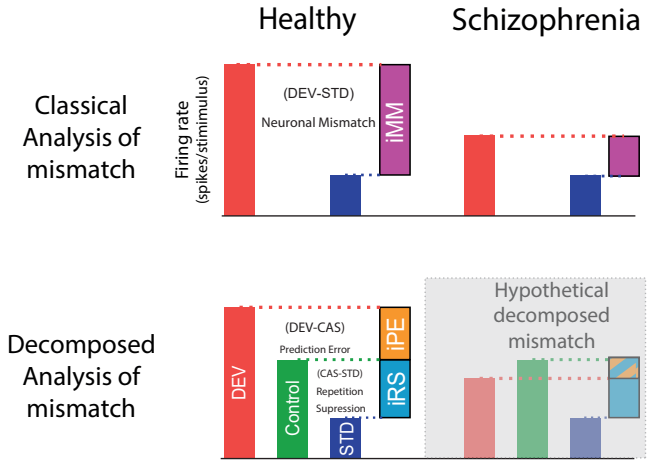

Figure 1. Experimental design. a) Frequency response area example, with a representation of the ten selected tones to build the experimental paradigms. **b)** Stimulation sequences, the same tone could be presented in different experimental paradigms, thus we can compare same tone in different contexts to control adaptation and deviance detection; and conform the indices of neuronal mismatch (iMM), prediction error (iPE) and repetition suppression (iRS). Note that ascending and descending tones will be compared to the control ascending or descending, respectively. **c)** Sketch of summary results of mismatch responses for healthy and schizophrenia subjects under the classical analysis of mismatch. Second row decomposition of neuronal mismatch, under the assumption of predictive coding framework in healthy subjects, and the hypothetical decomposition of neuronal mismatch into prediction error and repetition suppression in schizophrenia.

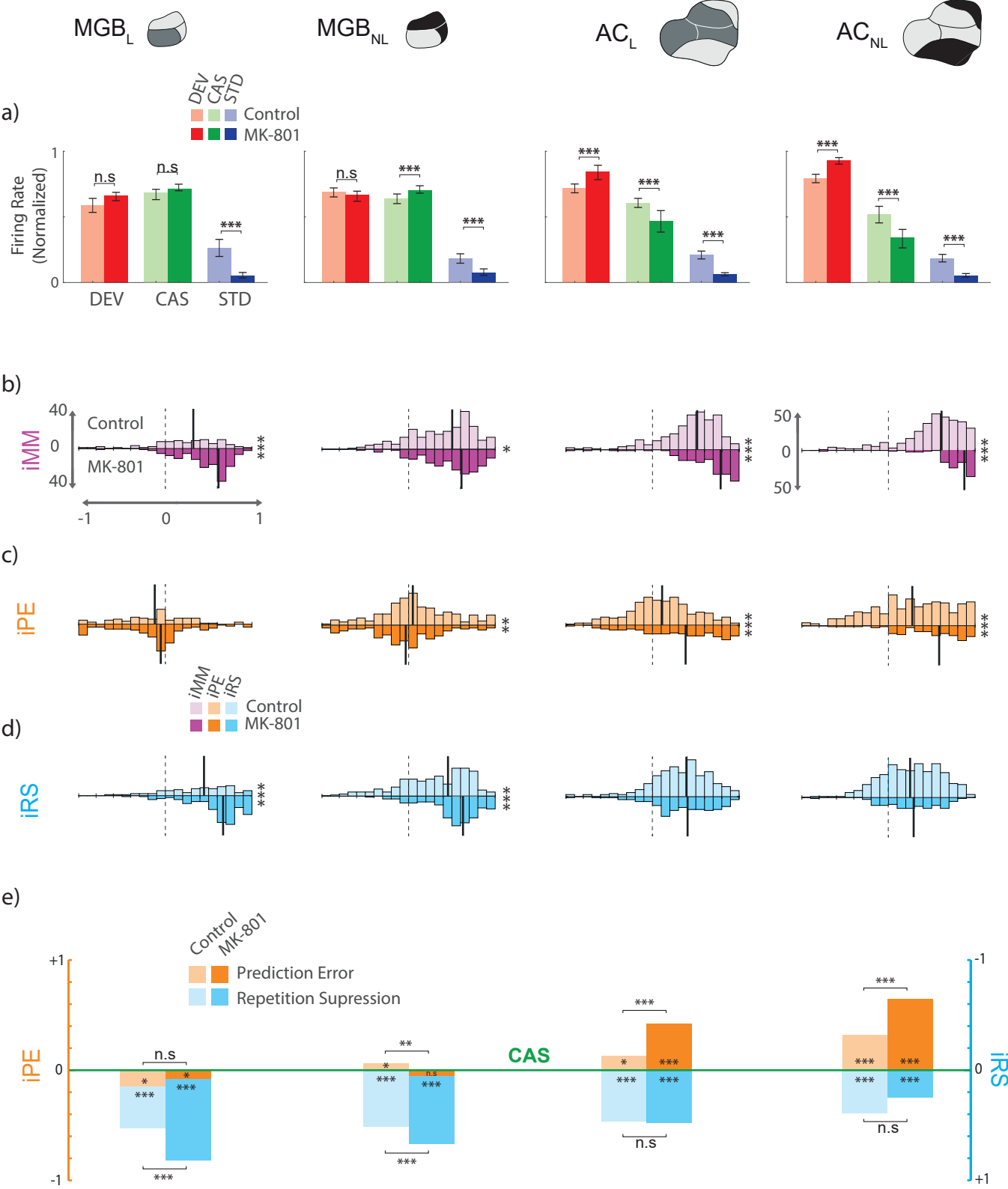
MGB_L
MGB_NL
AC_L
AC_NL
a)
DEV CAS STD
Control
MK-801
Firing Rate (Normalized)
1
0
n.s
***
DEV
CAS
STD
b)
iMM
40
0
40
Control
MK-801
-1
0
1
*
50
0
50
c)
iPE
**
d)
iRS
iMM iPE iRS
e)
Control MK-801
Prediction Error
Repetition Supression
+1
-1
CAS

Figure 2. **Single neuron spikes population analysis**. Results for firing rate analysis and their computed differences along the thalamocortical axis. **a)** Boxplot of median normalized responses for deviants (red), cascade (green) and standard (blue) for each group, control (light colors) and MK801 (bright colors), within each station and the statistical significance between groups (Wilcoxon signed-rank test, * $p<0.05$, ** $p<0.001$, *** $p<0.000$). **b-d)** Indices histograms displayed in a mirror-like manner for the two groups (controls upper and in light colors; MK801 under and in bright colors), showing the distribution of the three indexes for each neuronal response (ranging between -1 and +1, dotted lines indicate index=0). Vertical solid lines indicate their medians and the significant difference between groups is noted at the right of each histogram block. **e)** Median indices of Prediction Error (orange) and **d)** Repetition Suppression (blue), represented with respect to the baseline set by the cascade control (green line). Thereby, iPE upwards-positive while iRS is downwards-positive. Each median index corresponds to differences between normalized responses in a). Asterisks inside bars denote statistically significance of these indices against zero (Friedman test), while asterisks outside bars denote statistically significance between groups (Wilcoxon signed-rank test, * $p<0.05$, ** $p<0.001$, *** $p<0.000$).

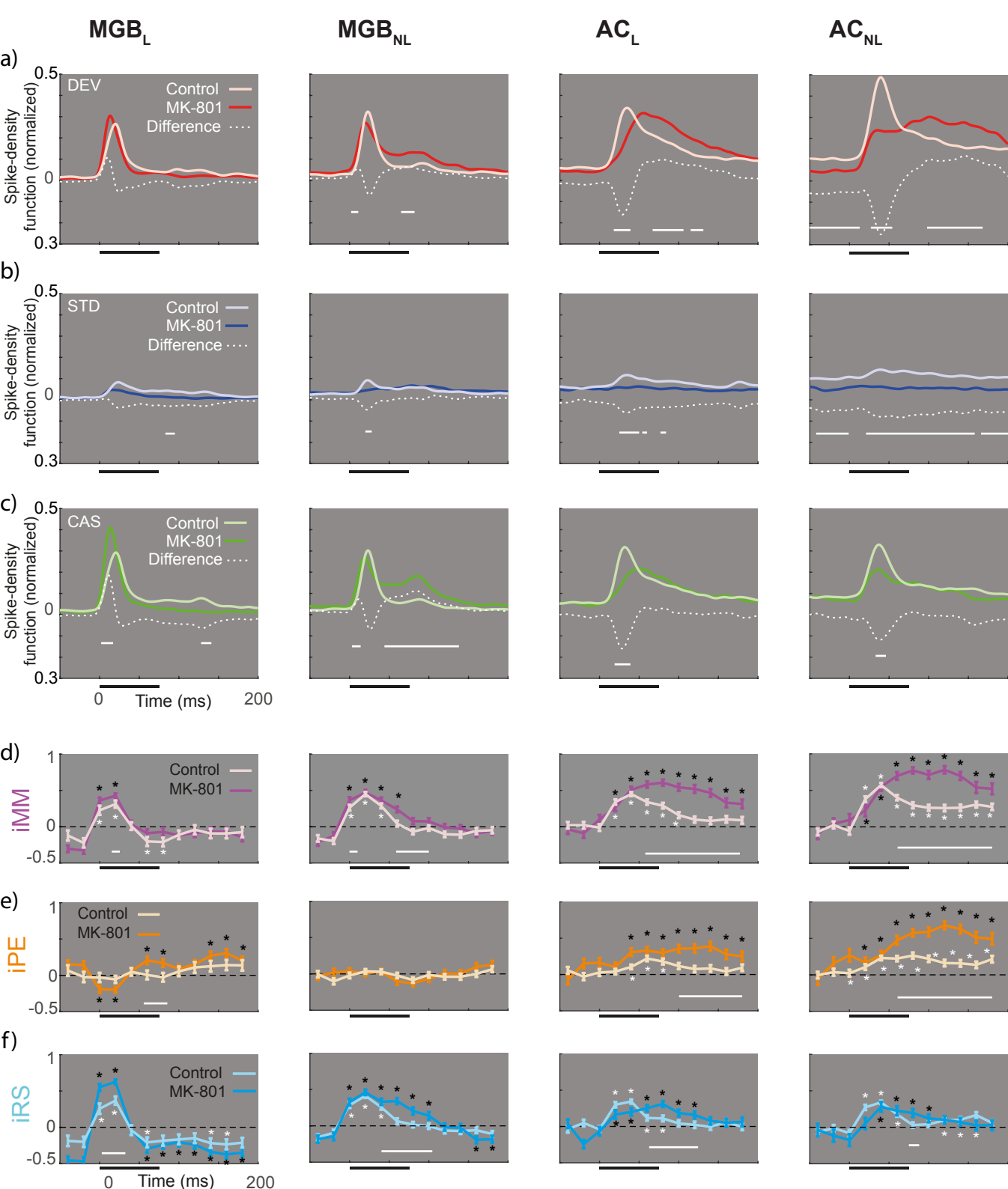
MGB_L
MGB_NL
AC_L
AC_NL
a)
DEV
Control
MK-801
Difference
Spike-density function (normalized)
0.5
0
0.3
b)
STD
Control
MK-801
Difference
Spike-density function (normalized)
0.5
0
0.3
c)
CAS
Control
MK-801
Difference
Spike-density function (normalized)
0.5
0
0.3
0
Time (ms)
200
d)
iMM
Control
MK-801
1
0
-0.5
e)
iPE
Control
MK-801
1
0
-0.5
f)
iRS
Control
MK-801
1
0
-0.5
0
Time (ms)
200

Figure 3. Spike Density Function. Peristimulus time histogram along the thalamocortical axis. **a-c)** Averaged firing rate profiles for each condition as normalized spike-density function (light colors for control and bright color for MK801 group), and their respective differences (white dotted lines). Solid horizontal white lines represent the time in which the difference between groups is significant (two-sample *t* test $p<0.05$, Bonferroni corrected). **d-f)** Indices over time computed for 12 intervals (from -50 to 190ms) compared against zero (signed-rank test and FDR corrected for 12 comparisons; * $p<0.01$) for each group (light colors for control and bright color for MK801 group). Solid white lines denote differences between groups across time intervalss (two-sample *t* test for each of the 12-time windows, $p<0.05$).

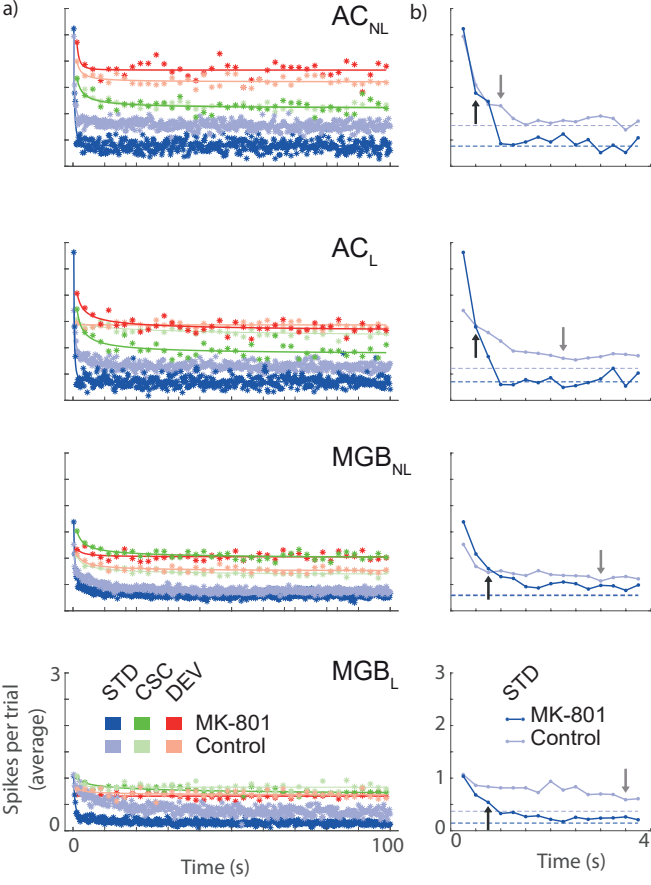
a)
b)
AC$_{NL}$
AC$_{L}$
MGB$_{NL}$
MGB$_{L}$
STD
CSC
DEV
MK-801
Control
Spikes per trial (average)
3
0
0
100
Time (s)
STD
MK-801
Control
3
2
1
0
0
4
Time (s)

Figure 4. Time course for dynamical thalamocortical adaptation. **a)** Averaged time course for the stimulus played in relation to the time elapsed from the beginning of the sequence. **b)** The first fifteen standard stimuli showing the three parameters of the power low fitted: *a* initial average response; *b* adaptation velocity; and *c* the steady-state value (dotted lines) for each group. Arrows represent the 50% of the initial responses demonstrating faster adaptation in the MK801 group and the break down in the dynamical hierarchy of adaptation.

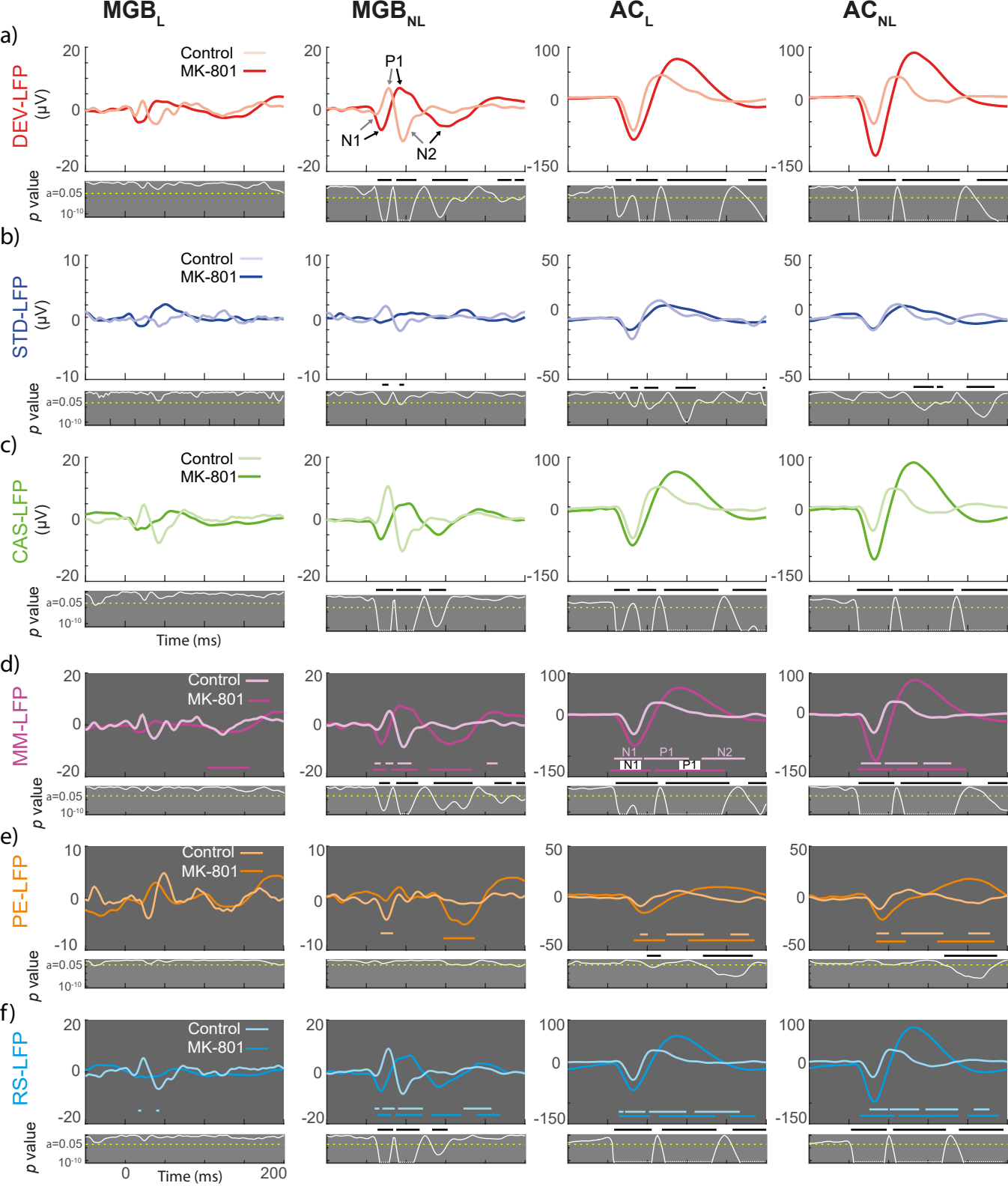
MGB_L
MGB_NL
AC_L
AC_NL
a)
DEV-LFP
(μV)
Control
MK-801
P1
N1
N2
p value
a=0.05
10^-10
b)
STD-LFP
c)
CAS-LFP
Time (ms)
d)
MM-LFP
e)
PE-LFP
f)
RS-LFP
0
200

Figure 5. Local Field Potentials for each condition and their differences. a-c) Population grand-averaged LFP for each condition recorded (CAS, DEV and STD) within each group (controls and MK801). Grey panels under the main LFP representations shows the instantaneous *p* value (white trace) of corresponding stimulus condition LFP (critical threshold set at 0.05 represented as a horizontal dotted yellow line). The thick black horizontal bars in figure 5a-c highlights the time interval for which the LFP comparison between the control and MK801 groups is significant. **d-f)** Population grand-averaged LFP for and neuronal Mismatch (MM-LFP=LFP_{DEV}-LFP_{STD}), Prediction Error (PE-LFP=LFP_{DEV}-LFP_{CAS}), and Repetition Suppression (RS-LFP=LFP_{STD}-LFP_{CAS}) respectively Colored horizontal lines denote significative deflections (*t*-test, FDR corrected). Grey panels show the instantaneous *p* value (white trace) of corresponding stimulus condition LFP (critical threshold set at 0.05 represented as a horizontal dotted yellow line) and black horizontal lines the time interval in which MK801 and control are statistically different.

a) Medial Geniculate Body Histology

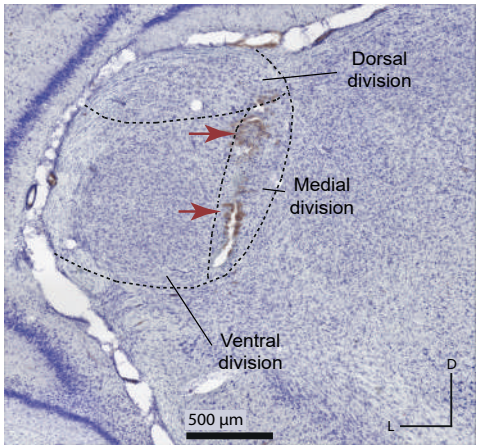

Bregma -5.7

b) Auditory Cortex Tonotopic mapping

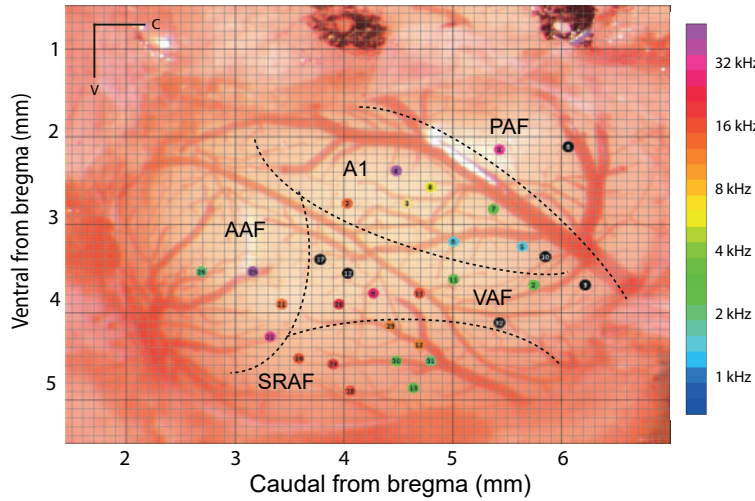

Figure 6. Anatomical recordings location. **a)** Photomicrography sample of a MGB Nissl-stained slice (10x), red arrows point the two electrolytic lesions. **b)** Example of localization all recordings made in the AC of one rat, each colored dot represent the characteristic frequency of each performed tract. A1: Primary Auditory Field; AAF: Anterior Auditory Field; VAF: Ventral Auditory Field; PAF: Posterior Auditory Field and SRAF: Suprarhinal Auditory Field.